RSC Advances

PAPER

View Article Online
View Journal | View Issue

Cite this: *RSC Adv.*, 2026, **16**, 27795

High-performance flexible electronics from organic fluorosilicone/carbon composites for low-temperature wearable sensors

Xiaoyu Ma, Yulu Wang* and Hongxia Zhu *

Flexible wearable sensors often fail in cold and wet environments due to the embrittlement of polymer substrates and the consequent interfacial delamination. Herein, we present a durable composite electrode material designed to overcome this "low-temperature brittleness" challenge. The material is fabricated by spray-coating a conductive carbon paste onto a substrate of organic fluorosilicone synthetic leather, which is synthesized *via* platinum-catalyzed hydrosilylation. With an optimal fluorosilicone oil content of 6 wt%, the composite film exhibits excellent mechanical properties (tensile strength: 14.83 MPa, elongation at break: 296.25%), remarkable hydrophobicity (water contact angle > 128°), and outstanding fatigue resistance. The resulting flexible sensor demonstrates a wide strain sensing range (0.5–20%), high sensitivity, a fast response time (~0.1 s), and exceptional long-term stability over 200 loading–unloading cycles. Crucially, these performances are well retained even at extremely low temperatures (*e.g.*, −80 °C). Additional interfacial, mechanical, and morphological characterization studies confirm strong adhesion between the conductive layer and the fluorosilicone substrate, as well as excellent mechanical stability under low-temperature conditions. SEM analysis further reveals that the formation of a continuous conductive network and controlled crack evolution under strain are responsible for the stable electromechanical performance. This work provides an effective material strategy for developing reliable wearable electronics capable of operating in harsh environments, with potential applications in health monitoring, human motion detection, and soft robotics.

Received 25th March 2026
Accepted 27th April 2026

DOI: 10.1039/d6ra02458k

rsc.li/rsc-advances

Introduction

In recent years, flexible wearable sensor devices have been widely applied in health monitoring, human motion detection, electronic skin, and human–machine interfaces.[1–4] However, as the ambient temperature decreases, the above-mentioned intelligent functions gradually weaken or even disappear; therefore, developing wearable devices that can operate stably under extreme low-temperature environments has become an urgent challenge.[5] At low temperatures, the glass transition of polymer substrates (such as polyurethane (PU) and polyethylene terephthalate (PET)) in flexible electronic devices is a key bottleneck leading to the failure of mechanical reliability. When the temperature drops below the glass transition temperature (T_g), the substrate materials undergo stiffening and embrittlement, and the large thermomechanical mismatch between the substrate and the conductive functional layers (such as metal films or printed conductive traces) induces severe interfacial stresses, ultimately leading to cracking, delamination of the conductive layers, and even complete failure of device functionality.[6–8] Moreover, in practical wearable applications, flexible devices are required to withstand long-term complex mechanical deformations such as bending and stretching, while being continuously exposed to harsh environmental factors including moisture, sweat permeation, and water vapor infiltration. These conditions can readily induce electrical resistance drift, interfacial instability, and even functional degradation of the conductive layers.[9–14] Notably, under low-temperature or extremely cold conditions, water vapor condensation and frosting can further aggravate interfacial delamination and electrical deterioration, severely limiting the reliable operation of flexible electronic devices in cold environments.[15,16] Therefore, developing or selecting flexible substrate or encapsulation materials that can maintain stable mechanical compliance over a wide temperature range (particularly at low-temperatures), while simultaneously providing effective waterproof and moisture-resistant protection and robust integration with functional layers, remains a critical challenge for advancing flexible electronics toward practical deployment, especially in extreme environments.[17–20]

Silicone polymers exhibit characteristics such as easy film formation, good aging resistance, resistance to high and low-temperatures, solvent resistance, flame retardancy, hydrophobicity, and excellent electrical insulation.[21] As an important branch of silicone materials, fluorosilicone polymers not only

Faculty of Light Industry, Qilu University of Technology (Shandong Academy of Sciences), Jinan 250353, China. E-mail: hxzhu@qlu.edu.cn

retain the excellent properties of conventional silicones but also exhibit lower surface energy and more stable chemical resistance, enabling reduced surface tension at coating–fabric interfaces and prolonged service life of oil- and solvent-resistant products. This makes it a highly promising passive flexible substrate material suitable for high-cold or variable-temperature environments.[22–25] The crosslinked network structure constructed *via* hydrosilylation is stable and can provide the necessary mechanical support and durability.[26] However, although fluorosilicone systems incorporating perfluoroalkyl side chains can achieve extremely low surfaceenergy and thus provide excellent waterproof performance, their high raw-material cost severely restricts large-scale applications. In contrast, the fluorosilicone component with trifluoropropyl (–$CH_2CH_2CF_3$) groups employed in this study enables a reduced fluorine content and lower cost while still delivering outstanding hydrophobicity, offering a feasible strategy for constructing high-performance waterproof flexible material systems suitable for low-temperature environments.[27,28] Although organic fluorosilicone materials themselves exhibit excellent low-temperature performance, constructing a conductive circuit on them that remains equally stable and reliable at low-temperatures is the key to achieving functional integration. From a mechanistic perspective, the performance of flexibleconductive materials at low temperatures strongly depends on both the polymer matrix properties and the conduction mechanism. Hydrogel-based sensors relying on ionic conduction are particularly vulnerable to freezing effects, while conventional polymer composites often suffer from reduced sensitivity due to matrix stiffening and interfacial instability.[29–31] In contrast, fluorosilicone-based systems offer distinct advantages. The Si–O backbone exhibits high flexibility and a low glass transition temperature, enabling the material to maintain mechanical compliance under extreme cold conditions. Moreover, the hydrophobic nature of fluorosilicone suppresses moisture-related effects, while the use of an electronically conductive network ensures stable electrical transport dominated by interparticle contact and tunnelling effects, which are less sensitive to temperature variations.[32–34] Therefore, the combination of a low-T_g fluorosilicone matrix and a stable conductive network provides an effective strategy for achieving reliable electromechanical performance under low-temperature conditions. Based on the above considerations, conductive carbon paste was selected as the conductive functional material in this study due to its stable electrical resistance, mature printing processes, low cost, and strong interfacial adhesion with elastomeric substrates.[35,36] By patterning the carbon paste onto the surface of the organic fluorosilicone substrate *via* spray coating and subsequent curing, a robust composite interface capable of withstanding low-temperature buckling is expected to be formed.[37]

This study aims to develop and systematically evaluate a composite flexible electrode based on organic fluorosilicone synthetic leather and spray-coated carbon paste, with a particular focus on its performance under low-temperature conditions. First, vinyl-functional fluorosilicone oil was prepared, followed by the fabrication of organic fluorosilicone synthetic leather *via* hydrosilylation, and flexible wearable sensors were then produced by spray-coating conductive carbon paste onto the coating surface. The effects of different fluorosilicone oil contents on the tensile strength, elongation at break, hydrophobicity, and wear resistance of the coatings were investigated, enabling optimized control over the physical properties of the silicone polymer coatings through adjustment of the fluorosilicone oil content. The electrical stability of the spray-coated carbon paste electrodes at room temperature and low-temperatures, as well as their fatigue resistance under repeated bending deformation, was also investigated. In addition, the effects of conductive carbon incorporation on mechanical properties, interfacial adhesion, durability, and low-temperature stability were systematically evaluated through tensile testing, long-term folding tests, and morphological characterization. Surface and interfacial microstructures before and after deformation under different temperature conditions were further analyzed to elucidate the relationship between morphology and performance. The experimental results demonstrate that this composite system significantly outperforms conventional PU-based electrodes, exhibiting great potential and reliability for low-temperature applications and providing an effective solution to the challenge of "low-temperature brittleness" in flexible electronic devices.

Results and discussion

Structure characterization of fluorosilicone oil and MTFPS

Fig. 1(a) shows the FTIR spectra of D_4, D_3F, and the product VTFPS. As can be seen, the C=C stretching vibration peak of the vinyl cyclic siloxane at approximately 1600 cm^{-1} is clearly observed in the fluorosilicone oil, indicating that the vinyl groups of the end-capping agent were successfully retained at the molecular chain ends. Compared with the sharp features of D_4 and D_3F, the Si–O–Si absorption band of the fluorosilicone oil around 1058 cm^{-1} is significantly enhanced and broadened, suggesting that both monomers underwent ring-opening copolymerization to form a linear siloxane backbone. In addition, the enhanced C–F absorption at 1204 cm^{-1} in the fluorosilicone oil confirms that fluorinated groups from D_3F were successfully incorporated into the polymer chain. Taken together, these spectral changes demonstrate that the target product VTFPS was successfully synthesized using D_4, D_3F, and the vinyl cyclic siloxane as reactants. In the ^1H NMR spectrum of VTFPS (Fig. S1), the multiplet observed at 5.75–6.10 ppm corresponds to the protons of the terminal vinyl groups. The presence of this set of signals unambiguously confirms that both ends of the polymer chains are capped with vinyl groups *via* propylene linkages (–CH_2–CH=CH_2), which is fully consistent with the designed molecular structure.

The FTIR spectra of the MTFPS polymers obtained in this study are shown in Fig. 1(b). Multiple stretching vibration absorption peaks can be observed, including the C–H stretching vibration at 2970 cm^{-1}, the Si–O stretching vibration at 1262 cm^{-1}, and the Si–H stretching vibration at 2161 cm^{-1}. The C=C bending vibration absorption at 802 cm^{-1} is also visible in the spectrum. In addition, the C–F stretching vibration

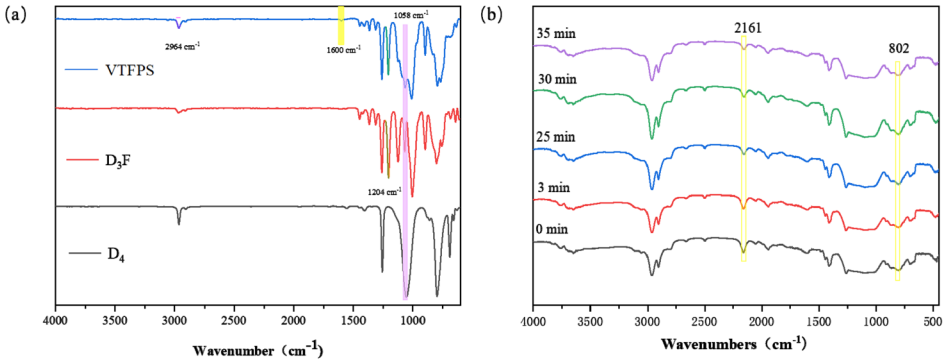

Fig. 1 (a) FT-IR spectrum of VTFPS; (b) FTIR spectra of MTFPS polymer films.

absorption at 1012.6 cm^{-1} is another prominent feature of the spectrum. Notably, the characteristic absorption peaks of the C═C bonds in the vinyl silicone oil at 802 cm^{-1} and the Si–H bonds in the hydride silicone oil at 2161 cm^{-1} are significantly reduced, indicating that a hydrosilylation reaction occurred between the C═C bonds of the vinyl silicone oil and the Si–H bonds of PMHS in the presence of the platinum catalyst. Overall, these results confirm that the reaction proceeded successfully and that the structure of the obtained product is consistent with the expected design.

Characterizations of MTFPS

To investigate the effect of different fluorosilicone oil contents on the final products, TGA was conducted to evaluate the thermal stability of the synthesized MTFPS-*x* polymers using a thermogravimetric analyzer. As shown in Fig. 2, when the weight loss reaches 10%, the corresponding decomposition temperature is 514 °C, and the maximum weight-loss rate occurs at 470 °C. Complete mass loss of the MTFPS polymer film is observed at approximately 680 °C. These results indicate that the MTFPS polymer films exhibit excellent thermal stability and outstanding high-temperature resistance.

The cold resistance of the synthetic leather coatings was characterized by measuring the glass transition temperature (T_g) of the polymer films. Fig. 3 presents the DSC curves of MTFPS polymers with different fluorosilicone oil contents (0 wt%, 3 wt%, and 9 wt%). As shown in the figure, the glass transition temperatures of the polymers with fluorosilicone oil contents of 0 wt%, 3 wt%, and 9 wt% are −85.6 °C, −82.9 °C, and −80.3 °C, respectively. All T_g values are below −80 °C, which can be attributed to the helical molecular structure of silicone polymers, the weak intermolecular interactions between chain segments, the soft and easily rotatable main chains, and the low rotational steric hindrance of the Si–C side groups.[38] These structural features endow polysiloxane molecular chains with excellent low-temperature flexibility. The results indicate that the coatings maintain outstanding flexibility and cold resistance at low-temperatures. Compared with conventional polymers such as PU and PVC, these coatings exhibit superior performance under low-temperature conditions, demonstrating their potential as materials for low-temperature applications.

Characteristics of MTFPS synthetic leather coatings

Based on the excellent low-temperature resistance of the MTFPS coatings, folding and flexing tests were conducted on MTFPS

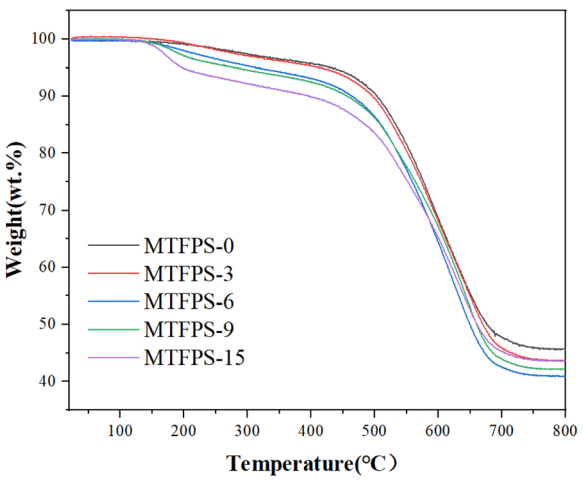

Fig. 2 TGA curves of polymers with different fluorosilicone oil contents (0 wt%, 3 wt%, 6 wt%, 9 wt%, and 15 wt%).

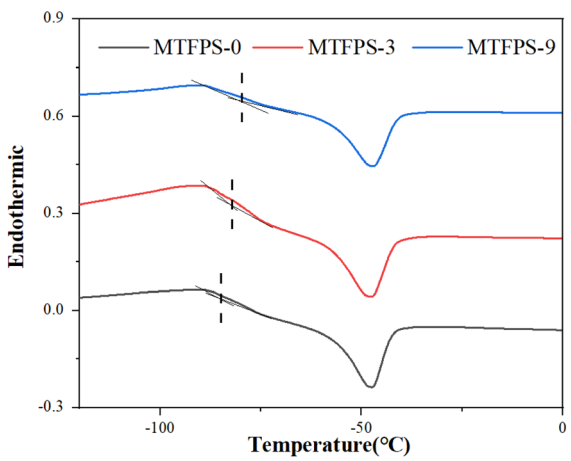

Fig. 3 DSC curves of polymers with different fluorine contents (0 wt%, 3 wt%, and 9 wt%).

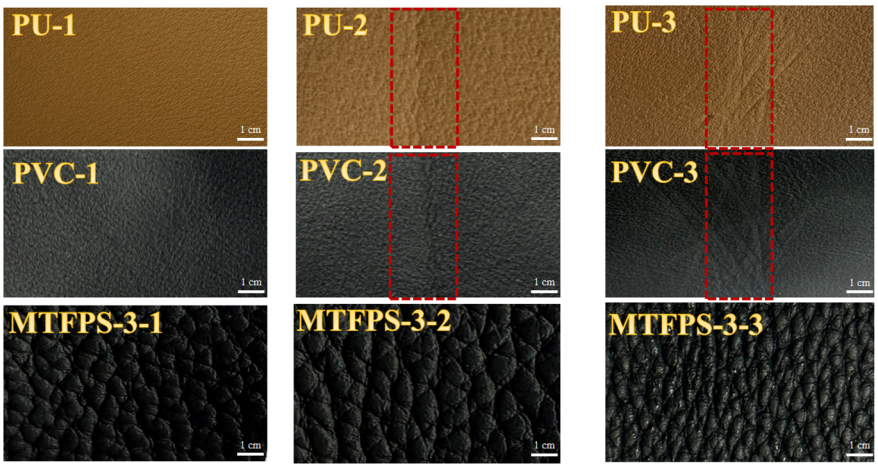

Fig. 4 Low-temperature flexibility tests of different leather coatings. X-1: pristine sample at room temperature; X-2: low-temperature folding crease test; X-3: low-temperature flexing test.

synthetic leather, PU, and PVC at low-temperature (−80 °C), and the results are shown in Fig. 4. Under low-temperature conditions, after 30 000 folding cycles, noticeable creases appeared on the surfaces of PU and PVC, whereas the surface of the MTFPS synthetic leather showed almost no change and exhibited only minimal differences compared with the pristine sample tested at room temperature. In the flexing test, the surfaces of the synthetic leathers were vigorously scratched with tweezers; pronounced scratches were observed on PU and PVC, while no obvious surface damage occurred on the MTFPS synthetic leather. These results further demonstrate that MTFPS synthetic leather possesses excellent low-temperature flexibility.

The hydrophobicity of the MTFPS synthetic leather coatings was characterized by measuring the water contact angle of the polymer coatings. Generally, coatings with lower surface energy and higher water contact angles exhibit better hydrophobic performance.[39] The contact angle measurements of coatings with different fluorosilicone oil contents at room temperature and low-temperature are shown in Fig. 5. The results indicate that, under both room-temperature and low-temperature conditions, the measured contact angles gradually increase with increasing fluorosilicone oil content, showing an overall upward trend. At both temperatures, the coating with a fluorosilicone oil content of 15 wt% exhibits the highest contact angles, reaching 128.3° and 130.1°, respectively, representing a significant improvement compared with the sample without fluorosilicone oil. This demonstrates that the introduction of low-surface-energy fluorinated groups effectively enhances the surface hydrophobicity of the material. Under low-temperature conditions, the contact angles of all materials show a slight increase.[40] Overall, the material exhibits excellent hydrophobic performance under both room-temperature and low-temperature environments, indicating good potential for anti-icing or low-temperature surface applications.

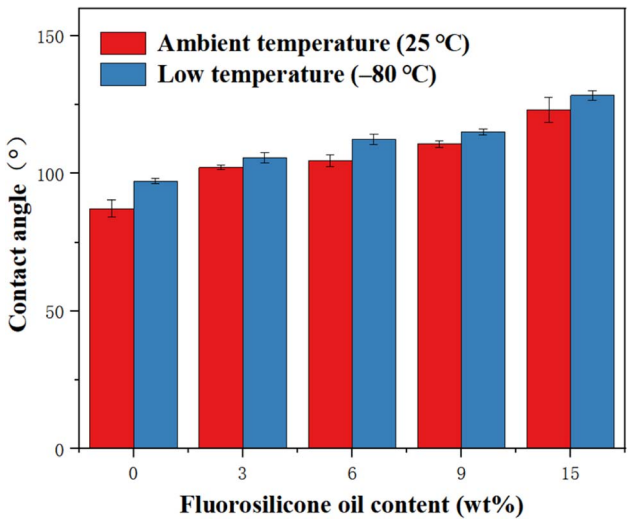

Fig. 5 Water contact angles of polymers with different fluorosilicone oil contents (0 wt%, 3 wt%, 6 wt%, 9 wt%, and 15 wt%) at room temperature and low-temperature.

Achieving durable anti-fouling performance in leather coatings remains a long-standing industrial challenge. Introducing fluorinated segments is an effective strategy to reduce surface energy, thereby increasing oil/water contact angles and suppressing the adhesion of contaminants such as inks.[41] As illustrated in Fig. 6, the anti-fouling behavior of the coating was systematically investigated by depositing typical staining liquids (coffee, ketchup, cola, soy sauce, and ink) onto the surface, followed by writing with black, blue, and red markers and ballpoint pens. After drying for 4 h, the surface was wiped with tissue paper. No visible residues or discoloration were observed, indicating that the MTFPS synthetic leather coating possesses outstanding anti-fouling performance.

As a coating material, appropriate strength and toughness are essential. The mechanical properties of the MTFPS synthetic leather coatings were tested, as shown in Fig. 7 The results indicate that when the fluorosilicone oil content is 3 wt%, the tensile strength reaches a maximum of 13.5 MPa, representing

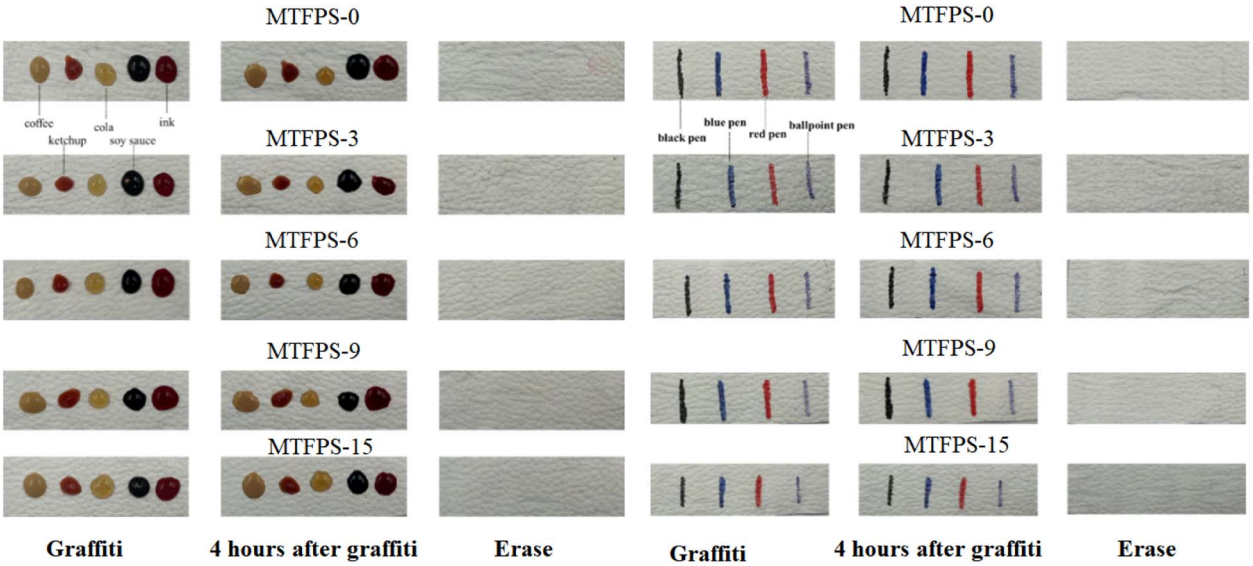

Fig. 6 Anti-fouling performance test results of MTFPS-3 synthetic leather coatings.

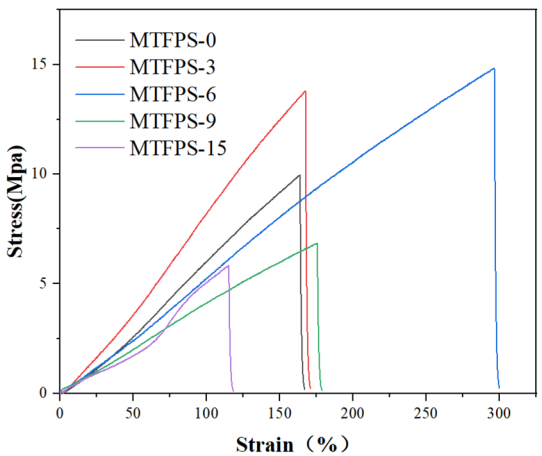

Fig. 7 Stress–strain curves of polymers with different fluorosilicone oil contents (0 wt%, 3 wt%, 6 wt%, 9 wt%, and 15 wt%).

an increase of approximately 32% compared with the fluorine-free sample. At 6 wt% fluorosilicone oil, the elongation at break reaches a maximum of 296.25%, demonstrating excellent flexibility. These results indicate that an appropriate amount of fluorosilicone oil can improve mechanical properties by introducing flexible chain segments, and the coatings meet the mechanical performance requirements for synthetic leather applications.

Products such as sofas and bags require leather with high wear resistance. Abrasion tests were conducted using a wear tester, and the wear resistance of the coatings was evaluated based on the wear index. As shown in Fig. 8, after the abrasion tests, all three samples exhibited some degree of surface wear. The wear index of theMTFPS-3 synthetic leather coating was calculated to be 160.9 cycles per mg, which is higher than that of PU leather (80.5 cycles per mg) and PVC leather (52.3 cycles per mg), indicating that the MTFPS synthetic leather coating demonstrates the best wear resistance. Generally, the wear resistance of polymer coatings is closely related to their strength, toughness, and resilience.[42] The Si–O–Si bonds in the polysiloxane main chain have large bond angles and bond lengths, making the molecular chains very flexible and endowing the polymer with excellent toughness and resilience. Consequently, the MTFPS synthetic leather coatings exhibit outstanding wear resistance.

Flexural endurance is an important indicator of leather softness. After 30 000 folding cycles, the surfaces of MTFPS-3 synthetic leather, PU, and PVC are shown in Fig. 9 The results

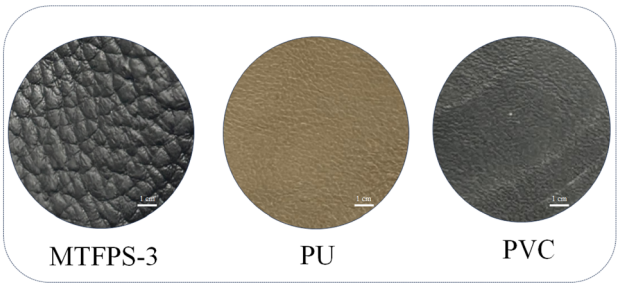

Fig. 8 Wear resistance tests of different leathers.

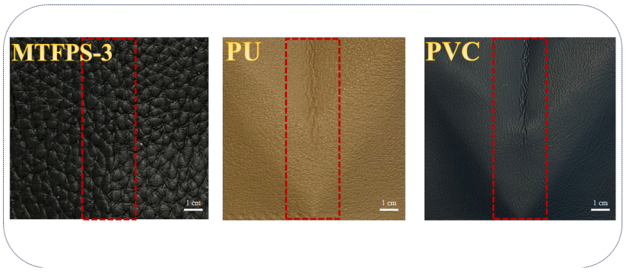

Fig. 9 Flexural endurance tests of different leathers.

indicate that MTFPS-3 synthetic leather maintained an intact surface structure, showing almost no creases and quickly recovering its original shape, demonstrating excellent fatigue resistance and shape-memory capability. Although PU possesses some flexibility, surface indentations were still observed, while PVC, due to its high rigidity and poor toughness, exhibited obvious cracks and peeling under high-frequency folding stress.[43,44] As shown in the SI (Fig. S2 and 3), MTFPS synthetic leathers with varying fluorosilicone oil contents exhibited only negligible surface creasing after 30 000 folding cycles at both 25 °C and −80 °C, demonstrating outstanding flexural durability under ambient and ultralow-temperature conditions. These results further highlight that the rational incorporation of fluorosilicone components markedly enhances the flexuralendurance of synthetic leather, enabling its potential application in scenarios involving repetitive mechanical deformation, such as wearable electronics, seating materials, and electronic leather.

Finally, this study investigated the significant effects of different fluorosilicone oil contents on the air permeability, water vapor transmission, and tear strength of MTFPS synthetic leather. The air permeability, water vapor transmission, and tear strength of MTFPS synthetic leather (Fig. S4 and 5) all first increased and then decreased with increasing fluorosilicone oil content. When the fluorosilicone oil content increased from 0 wt% to 6 wt%, the water vapor transmission rate rose from approximately 53.4 mL $(cm^2\ h)^{-1}$ to a peak of about 61.2 mL $(cm^2\ h)^{-1}$, while the air permeability increased rapidly from approximately 0.0078 mg $(cm^2\ h)^{-1}$ to a maximum of around 0.025 mg $(cm^2\ h)^{-1}$. The tear strength reached a maximum of 70.2 N mm^{-1} at 3 wt% fluorosilicone oil, representing an improvement of about 24% compared with the fluorine-free sample. These results indicate that the appropriate incorporation of fluorosilicone oil can effectively enhance the material's air permeability, moisture permeability, and tear strength.

Electrical conductivity of the coatings

After the incorporation of conductive materials, sensitivity becomes an indispensable performance feature of MTFPS synthetic leather in flexible wearable electronic devices, endowing it with broad potential for applications in piezoresistive strain sensors. In this study, the MTFPS sample with a fluorosilicone oil content of 9 wt% was selected as a representative composition for electromechanical performance evaluation. The dynamic electromechanical response of the material was systematically investigated through real-time measurements of relative resistance changes. As shown in Fig. 10(a) and (b), during repeated stretching cycles at small strains (0.5–3%) and moderate strains (5–20%), MTFPS synthetic leather exhibited stable resistance responses, demonstrating excellent sensing repeatability and reliability. Notably, the material is capable of detecting strains as low as 0.5%, indicating an extremely low detection limit, which enables it to monitor subtle human motions such as pulse and micro-muscle movements.

In addition, Fig. 10(c) shows the effect of different stretching rates (50–250 mm min^{-1}) on the resistance response of MTFPS synthetic leather under the same strain. The results indicate that, regardless of the loading rate, the output signals of the material remain regular and clear, with the cycle density changing according to the stretching frequency. This demonstrates that the material possesses excellent frequency response characteristics and a high sensitivity to dynamic strain variations, which is essential for achieving precise motion monitoring.

Fig. 10(d) further highlights the rapid response characteristics of the material. Under a 5% strain held for 3 seconds, the response time and recovery time were measured as 0.11 s and 0.12 s, respectively, indicating that the material can quickly sense external stress and recover promptly, meeting the high demands for real-time and continuous monitoring in flexible wearable devices.

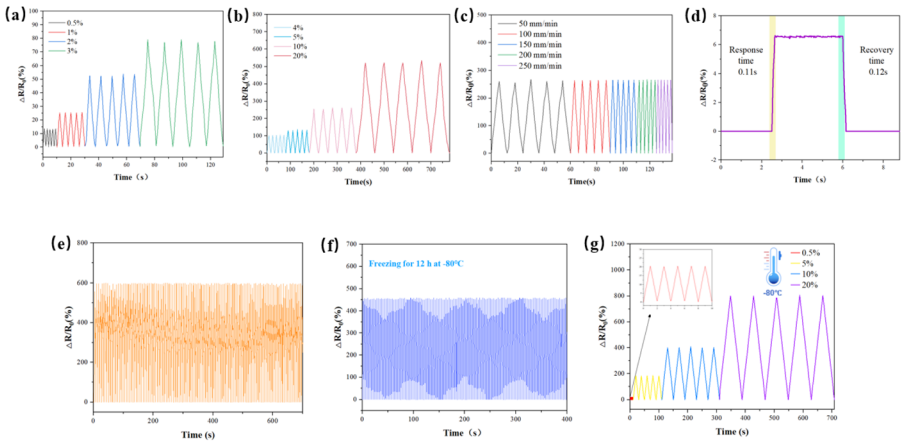

Fig. 10 (a) Relative resistance changes under small strains of 0.5–4%; (b) relative resistance changes under moderate strains of 5–40%; (c) relative resistance changes at different stretching frequencies; (d) rapid response and recovery times under 5% strain; (e) relative resistance changes over 200 stretch-release cycles at a constant 20% strain; (f) relative resistance changes over 200 stretch-release cycles at 0% strain after 12 hours of freezing; (g) sensing performance under different tensile strains at −80 °C.

To evaluate the stability and applicability of the MTFPS conductive coating under extreme conditions, comparative tests were conducted on its resistance response after storage at room temperature and freezing at −80 °C for 12 hours. As shown in Fig. 10(e) and (f), the material underwent 200 cycles of stretch-release loading under both temperature conditions. To ensure stable and reliable signal acquisition under different temperature conditions, the experimental parameters and acquisition time windows were appropriately adjusted according to the response characteristics of the material; therefore, the total testing durations are not identical for the two measurements. The results show that at a constant 20% strain, the fluorosilicone synthetic leather exhibits excellent sensing stability and signal reversibility, with R/R_0 values maintained between 400% and 600% at room temperature, showing clear waveforms and good periodicity, with only minor drift in localized regions. The frozen samples at −80 °C were also able to complete 200 cycles, with R/R_0 stabilized around 460% and negligible baseline drift, showing highly consistent cyclic behavior.

These results clearly demonstrate that the MTFPS conductive coating can maintain a stable conductive network and structural integrity even under extreme low-temperature conditions, reflecting outstanding low-temperature mechano-electrical stability and durability. The anti-freezing capability of the material can be attributed to the flexible main-chain structure of the polysiloxane network in its matrix, which inherently provides excellent low-temperature flexibility and resistance to freeze-induced cracking. Consequently, synthetic leather composed of this material can continue to output stable electrical signals even after being frozen at −80 °C for 24 hours, demonstrating exceptional environmental adaptability and signal recovery performance.

Furthermore, as shown in Fig. 10(g), to investigate the strain-response behavior at low-temperatures, cyclic strains of 0.5%, 5%, 10%, and 20% were applied to the samples in a −80 °C environment. All measurements were conducted in a temperature-controlled chamber at −80 °C after sufficient thermal equilibration. Cyclic tensile tests were performed under continuous loading–unloading conditions at a fixed strain without any intentional holding time, while the electrical resistance was continuously recorded using a digital source meter. The results show that with increasing strain amplitude, R/R_0 increases significantly, reaching approximately 30%, 170%, 400%, and 800%, respectively, exhibiting a good linear response. It should be noted that the higher resistance variation observed in Fig. 10(g), compared to that in Fig. 10(f) at the same strain level, is mainly attributed to differences in the mechanical history and fatigue state of the samples. During repeated cycling, partial structural rearrangement and fatigue of the conductive network lead to the formation of more stable conductive pathways, resulting in a relatively reduced resistance variation, as observed in Fig. 10(f). In contrast, the sample in Fig. 10(g), which experienced less prior cyclic loading, exhibits a more pronounced resistance response under the same strain. The MTFPS conductive coating not only demonstrates excellent strain sensitivity and cyclic stability at room temperature but also maintains outstanding electrical responsiveness and environmental adaptability under the extreme low-temperature condition of −80 °C. These properties highlight its broad potential and practical value for applications in flexible wearable sensors, polar wearable devices, human motion monitoring, and soft robotics.

Polysiloxane materials are widely regarded as ideal candidates for constructing next-generation flexible electronic devices—especially strain and pressure sensors—due to their skin-like extensibility and elasticity, excellent strain sensitivity, fatigue resistance, and electrical performance.[45] In this study, flexible sensing coatings based on MTFPS conductive polymers were developed for monitoring a variety of human motion signals, demonstrating strong practical applicability. As shown

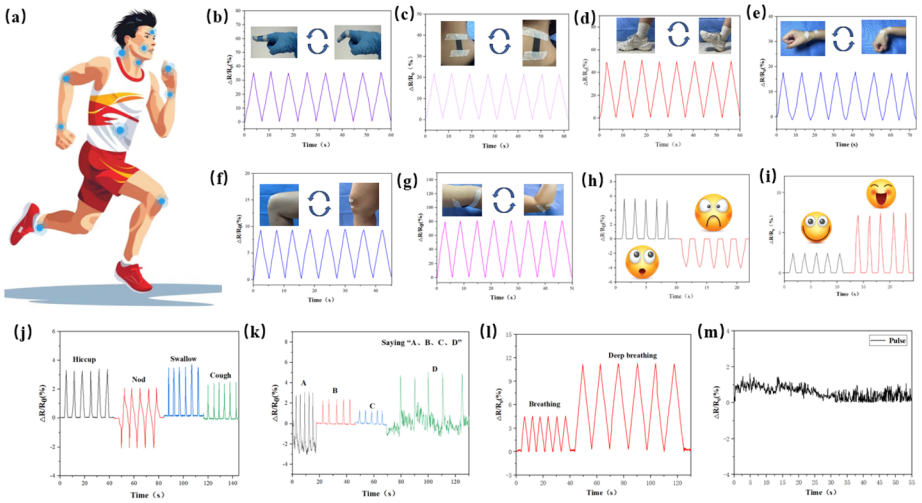

Fig. 11 Relative resistance changes of the MTFPS-9/C conductive coating as a strain sensor for monitoring various human motions: (a) different detection positions; (b) finger flexion and extension; (c) neck flexion and extension; (d) ankle dorsiflexion; (e) wrist flexion; (f) knee flexion; (g) elbow flexion; (h) smile and laughter; (i) frown and surprise; (j) hiccup, nod, swallow and cough; (k) voice recognition of different letters (*e.g.*, "A–D"); (l) shallow and deep breathing; (m) physiological signals of pulse variations.

in Fig. 11, the sensors can be conveniently attached to highly mobile regions such as fingers, wrists, elbows, knees, and ankles toidentify different movement states. Fig. 11(b) shows that during repeated finger bending, the device outputs highly periodic and reproducible electrical signals (R/R_0) with clear and stable waveforms, enabling accurate detection of bending frequency and amplitude variations.

Fig. 11(c–g) further illustrates the sensor's performance in monitoring neck flexion and ankle, wrist, knee, and elbow movements. The $\Delta R/R_0$ signal fluctuates within ranges of 20–130%, with peaks distributed regularly, responding rapidly without significant baseline drift. These results indicate that the coating maintains excellent electromechanical coupling stability and reliable signal output even under large-strain deformations and skin-bending conditions.

As shown in Fig. 11(h–m), this set of images systematically demonstrates the outstanding performance of the MTFPS conductive coating in sensing a variety of subtle human motions and physiological signals, including facial expression recognition, throat movement monitoring, speech recognition, breathing analysis, and pulse detection. These results fully validate its feasibility and broad potential as a flexible wearable device for health monitoring applications.

For facial expression recognition, attaching the MTFPS conductive coating to the facial skin allows clear differentiation between expressions such as "frowning" *vs.* "surprised" and "smile" *vs.* "laugh." The corresponding electrical signal waveforms are clear, respond rapidly, and show good repeatability, demonstrating excellent sensitivity to subtle muscle displacements. This feature highlights its key application potential in intelligent wearable devices for expression recognition, human–computer interaction, and emotion monitoring.

For throat movement monitoring, the MTFPS synthetic leather can successfully detect subtle actions such as swallowing, hiccupping, nodding, and coughing, producing distinguishableresistance signal waveforms. This indicates its stable responsiveness to complex micro-deformations in the throat region. In speech recognition tests, the pronunciation of different letters (*e.g.*, "A–D") generates distinct vibration patterns at the vocal cords, all of which were effectively captured by the sensor. This demonstrates its potential for use in assistive devices or silent speech interaction systems. Regarding respiration monitoring, the MTFPS synthetic leather can reliably distinguish between shallow and deep breathing states, showing excellent dynamic respiratory sensing capability. This functionality could be further applied in scenarios such as sleep apnea monitoring, exercise training, and chronic disease management.

To further demonstrate the practical application potential of the MTFPS conductive coating in intelligent human–machine interaction, it was applied to capacitive touch devices for operational testing. As shown in Fig. 12(a and b), the MTFPS conductive coating enables smooth and continuous handwriting input on a smartphone screen, including letters (*e.g.*, "QLU") and complex shapes (*e.g.*, stars, smiley faces, and suns), demonstrating excellent touch response performance and accurate trajectory reproduction. In addition, the coating can accurately perform call-dialing operations, completing the entire process from number input to call connection, confirming its high touch recognition accuracy and operational stability.

After being stored for five months, the electrical performance of the samples was re-evaluated to assess their long-term stability. As shown in Fig. 13(a), the cyclic resistance responses under tensile strains of 2%, 5%, 10%, and 20% were recorded, while the resistance variation during finger-bending deformation is presented in Fig. 13(b). Notably, the samples still exhibited excellent conductivity with highly regular and reproducible resistance changes under different deformation conditions, indicating negligible degradation of the conductive performance over time and confirming their outstanding long-term stability.

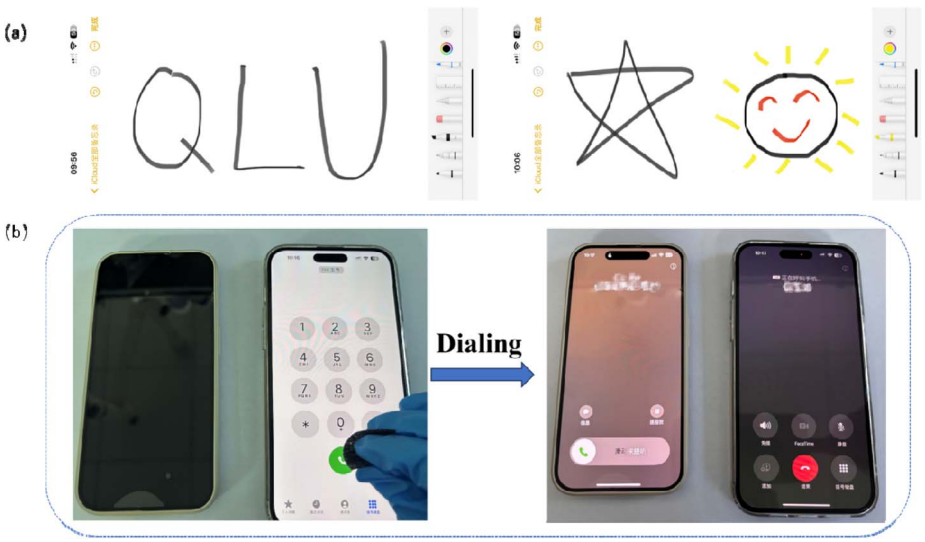

Fig. 12 (a) Handwriting "QLU" and drawing patterns such as a star and smiley sun; (b) dialing a phone number on a smartphone screen.

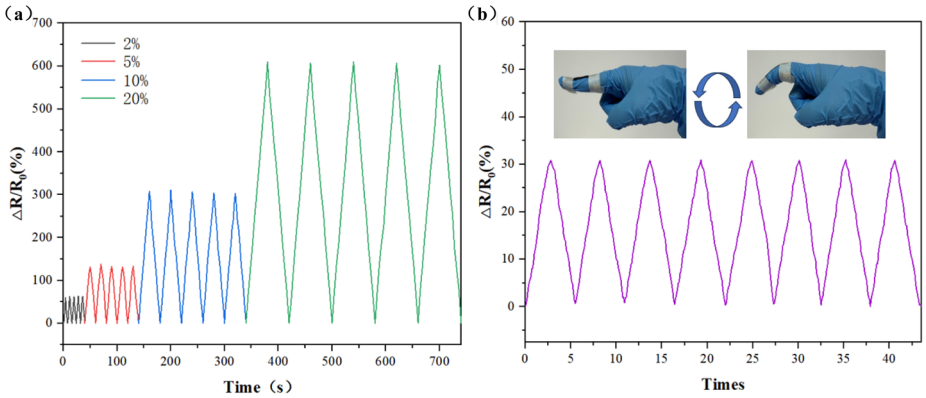

Fig. 13 (a) Cyclic $\Delta R/R_0$ responses under tensile strains of 2%, 5%, 10%, and 20% after 5 months of storage; (b) $\Delta R/R_0$ response during finger bending after 5 months of storage.

In summary, the MTFPS conductive coating not only enables precise detection of a variety of physiological signals, including facial expressions, throat movements, respiration, and pulse, but also demonstrates excellent stability, repeatability, and mechanical conformity. These features highlight its broad application potential in flexible wearable devices for intelligent health monitoring, human–machine interaction, rehabilitation, and assistive communication, making it particularly suitable for real-time, continuous sensing and feedback of human health and motion states.

To evaluate the interfacial adhesion between the conductive carbon layer and the fluorosilicone coating, a peeling test was performed, as shown in Fig. 14(a and b). The MTFPS-9 coating was first applied onto the leather substrate, followed by spray-coating of conductive carbon paste and subsequent thermal curing to form an integrated structure (Fig. 14(a)).

As shown in Fig. 14(b), during the peeling process, no obvious delamination was observed between the conductive carbon layer and the MTFPS-9 coating. Instead, the bonded structure remained intact, indicating strong interfacial adhesion between the two layers.

Further evidence is provided by the cross-sectional SEM image (Fig. 14(c)), where a compact and continuous interface can be clearly observed without noticeable gaps or separation. The conductive carbon layer is tightly integrated with the MTFPS-9 coating, suggesting effective interfacial bonding.

The strong adhesion can be attributed to the good interfacial compatibility between the MTFPS-9 matrix and the carbon paste, as well as the infiltration and mechanical interlocking that occur during the spray-coating and curing processes.

These results demonstrate that the incorporation of conductive carbon materials does not compromise interfacial integrity, but instead forms a robust composite structure, which

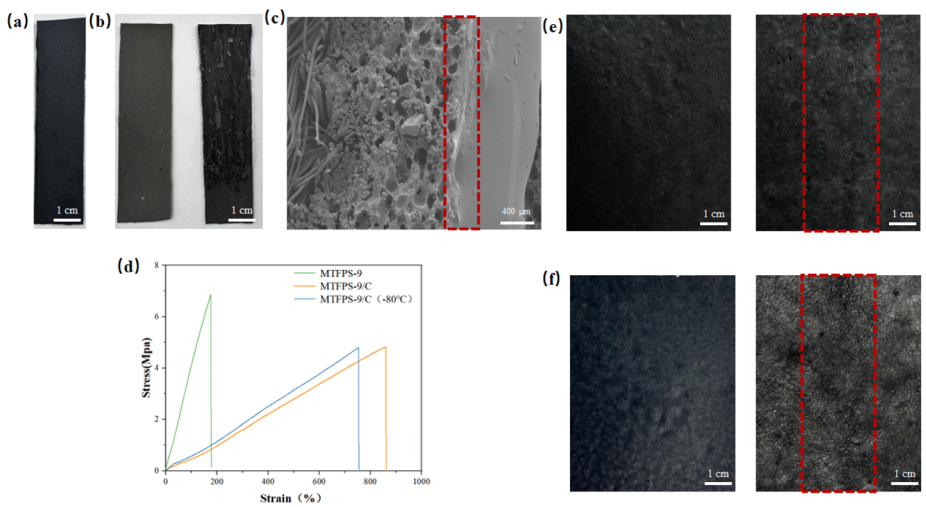

Fig. 14 (a) Photograph of the MTFPS-9 fluorosilicone coating on a leather substrate after spray-coating of conductive carbon paste and thermal curing; (b) photographs of the peeling test of the MTFPS-9/carbon composite sample; (c) cross-sectional SEM image of the interface between the conductive carbon layer and the MTFPS-9 coating; (d) stress–strain curves of MTFPS-9 (without conductive carbon materials), MTFPS-9/C at room temperature, and MTFPS-9/C at −80 °C; (e) surface morphology of MTFPS-9/C after 30 000 folding cycles at room temperature; (f) surface morphology of MTFPS-9/C after 30 000 folding cycles at −80 °C.

is essential for ensuring stable electrical performance under mechanical deformation and low-temperature conditions.

To systematically evaluate the effects of conductive carbon incorporation on the mechanical properties, durability, and low-temperature stability of the material, a series of mechanical and electromechanical tests were conducted, as shown in Fig. 14(d–f).

As shown in Fig. 14(d), tensile tests were performed on MTFPS-9 (without conductive carbon materials) and carbon-modified samples at room temperature, as well as carbon-modified samples at −80 °C (MTFPS-9/C, MTFPS-9/C(−80 °C)). The pristine MTFPS-9 sample exhibits relatively higher tensile strength but limited elongation. After the incorporation of conductive carbon materials, the tensile strength slightly decreases, while the elongation at break increases, indicating improved toughness and flexibility. Importantly, the stress–strain behaviour of MTFPS-9/C at room temperature and −80 °C is comparable, suggesting that the mechanical properties are well preserved under low-temperature conditions and demonstrating good mechanical stability.

The cyclic stretch-release behaviour (200 cycles), as previously shown in Fig. 10(e) and (f), further demonstrates the stable and repeatable resistance responses at both room temperature and −80 °C, indicating good cyclic stability and robustness of the conductive network.

In addition, repeated folding tests (30 000 cycles) were conducted at both room temperature and −80 °C to assess flexibility and structural durability, as shown in Fig. 14(e and f). At room temperature, the MTFPS-9/C samples show negligible surface changes after 30 000 folding cycles, whereas slight surface damage can be observed for the samples tested at −80 °C, as highlighted in the marked regions. Despite these minor changes, the overall structure remains intact, indicating that the material maintains good flexibility and structural stability even under extreme low-temperature conditions. The slight surface damage observed at low temperature is attributed to increased local stress concentration during deformation, which is consistent with the mechanical behaviour discussed above.

Overall, these results provide a systematic evaluation of the effects of conductive carbon incorporation on the mechanical properties, durability, and low-temperature stability of the material, thereby supporting the improved performance of the strain sensor.

The surface morphology of the samples was systematically investigated by SEM, as shown in Fig. 15. The pristine MTFPS-9 (Fig. 15(a)) exhibits a porous structure with numerous microvoid-like features, which can be attributed to the rapid evaporation of dichloromethane during the film-forming process. After the incorporation of conductive carbon materials, the MTFPS-9/C sample (Fig. 15(b)) shows a more continuous surface with distributed microstructural features, indicating the formation of a conductive network.

To further clarify the morphology–performance relationship, SEM observations were carried out at different magnifications (1 mm and 50 μm) under both room temperature and −80 °C conditions, before and after tensile deformation (Fig. 15(c–j)). For clarity, the images are arranged according to temperature and deformation state. Before stretching (Fig. 15(c–f)), the surfaces remain relatively uniform without visible cracks at both temperatures. At the millimetre scale (Fig. 15(c) and (e)), the coatings exhibit macroscopic roughness, which is attributed to the spray-coating process and thickness variation. At higher magnification (Fig. 15(d) and (f)), distributed microstructural features associated with solvent evaporation and phase separation can be observed. After tensile deformation (Fig. 15(g–j)), microcracks are generated and propagate along the surface due to stress concentration. These cracks disrupt and reconstruct the conductive pathways, thereby governing the

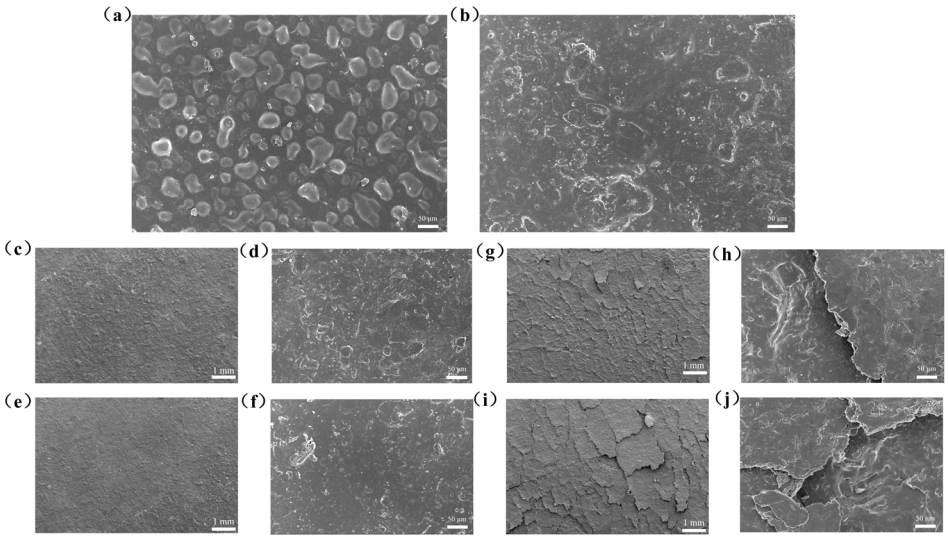

Fig. 15 (a) SEM image of the pristine MTFPS-9 sample; (b) SEM image of the MTFPS-9/C sample; (c, and e) SEM images of MTFPS-9/C before stretching at 1 mm scale under room temperature and −80 °C, respectively; (d, and f) SEM images of MTFPS-9/C before stretching at 50 μm scale under room temperature and −80 °C, respectively; (g, and i) SEM images of MTFPS-9/C after stretching at 1 mm scale under room temperature and −80 °C, respectively; (h, and j) SEM images of MTFPS-9/C after stretching at 50 μm scale under room temperature and −80 °C, respectively.

electromechanical response of the material. Notably, the crack morphology and distribution at −80 °C are comparable to those at room temperature, indicating that no significant brittle fracture occurs under low-temperature conditions. This suggests that the MTFPS-9 matrix maintains sufficient flexibility to preserve structural integrity and conductive network stability even at −80 °C.

Overall, the formation of a continuous conductive network combined with controlled crack evolution under strain establishes a clear morphology–performance relationship, accounting for the stable electromechanical behaviour and excellent low-temperature reliability of the material.

Experimental

Materials and methods

Octamethylcyclotetrasiloxane (D_4) was purchased from Shanghai Sigma-Aldrich Trading Co., Ltd (3,3,3-trifluoropropyl) methylcyclotrisiloxane (D_3F) was supplied by Guangzhou Yuanda New Material Co., Ltd Tetramethylammonium hydroxide (TMAH) was obtained from Shanghai Macklin Biochemical Technology Co., Ltd Conductive carbon paste (CH-8) was sourced from Guangdong Guangxin New Material Co., Ltd PU synthetic leather was procured from Anhui Anli Material Technology Co., Ltd, and PVC synthetic leather was provided by Zhejiang Yuanlong New Material Co., Ltd Karstedt's catalyst (platinum-divinyltetramethyldisiloxane complex, Pt ∼0.5%) was acquired from Dongguan Chengyin Silicone Technology Co., Ltd Divinyl-terminated polydimethylsiloxane ($^{Vi}PDMS^{Vi}$), divinyl-terminated poly(methylvinylsiloxane) ($^{Vi}PMVS^{Vi}$), and poly(methylhydrosiloxane) (PMHS) were all purchased from Jiangsu Tianchen New Material Co., Ltd

Synthesis of vinyl-functionalized fluorosilicone oil

The reaction scheme is shown in Fig. 16. The D_4 cyclic monomer was charged into a reaction flask and heated to 60–90 °C under reduced pressure for dehydration over approximately 1 hour. After releasing the vacuum, a pre-mixed amount of D_3F, TMAH, and $^{Vi}PDMS^{Vi}$ was added proportionally. The mixture was then heated to 100–120 °C under atmospheric pressure and

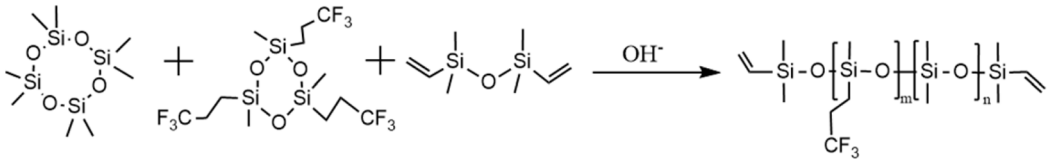

Fig. 16 Reaction scheme for the preparation of VTFPS.

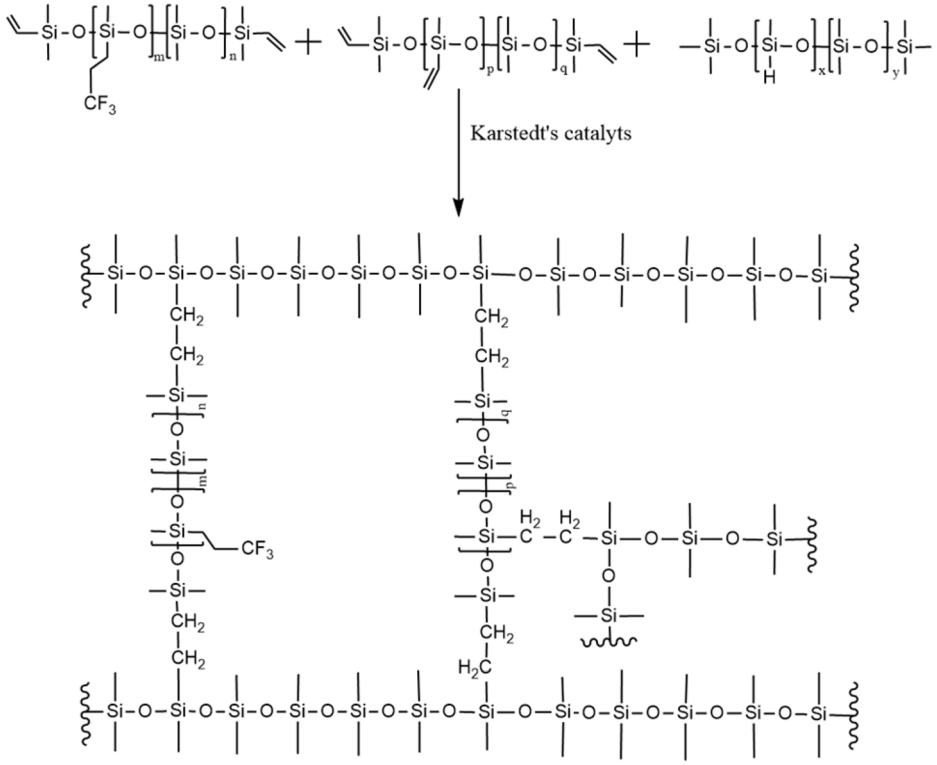

Fig. 17 Preparation scheme of MTFPS polymer film.

maintained at this temperature for 1 hour. Subsequently, the temperature was raised to 140–160 °C and held for an additional hour to facilitate the reaction. Upon completion, low-boiling fractions were removed under reduced pressure at 150–180 °C. The reaction was cooled to room temperature after the volatiles met the required specifications, yielding a colorless, highly viscous liquid, identified as Divinyl-terminated trifluoropropyl silicone oil (VTFPS).

Fabrication of MTFPS polymer films

As shown in Fig. 17, ^{Vi}PMVS^{Vi}, PMHS, and VTFPS with different mass fractions were first mixed uniformly in a beaker and then placed in a vacuum oven for degassing under reduced pressure for 15 min. After that, a platinum catalyst was added to the mixture and stirred thoroughly. The resulting mixture was blade-coated onto release paper using a coating bar. Subsequently, the release paper carrying the organic fluorosilicone slurry was thermally cured in an oven to obtain organic fluorosilicone polymer layers containing different mass fractions of VTFPS. The polymers were designated as MTFPS-x, where x represents the mass fraction of the VTFPS (x = 0–15 wt%).

Fabrication of MTFPS synthetic leather

As shown in Fig. 18, MTFPS synthetic leather was prepared by a dry transfer coating method. Release paper was used as the carrier, onto which the mixed slurry was coated. The organic fluorosilicone slurry was then thermally cured in an oven, followed by the application of a silicone adhesive. After the adhesive became semi-dry, the MTFPS polymer coating was laminated with the base fabric and heated in an oven. Finally, the release paper was peeled off to obtain MTFPS synthetic leather.

Fabrication of MTFPS Synthetic Leather for Wearable Sensing Devices

As shown in Fig. 19, first, ^{Vi}PMVS^{Vi}, PMHS, and VTFPS with different mass fractions were uniformly mixed in a beaker and placed in a vacuum oven for degassing under reduced pressure for 15 min. A platinum catalyst was then added to the mixture

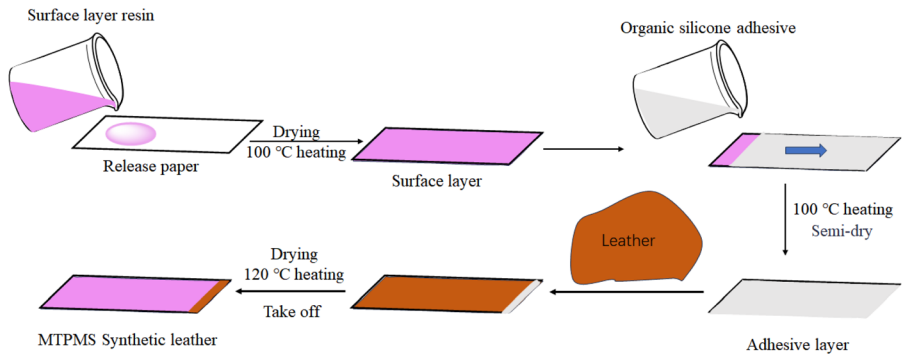

Fig. 18 Schematic illustration of the fabrication process of MTFPS synthetic leather.

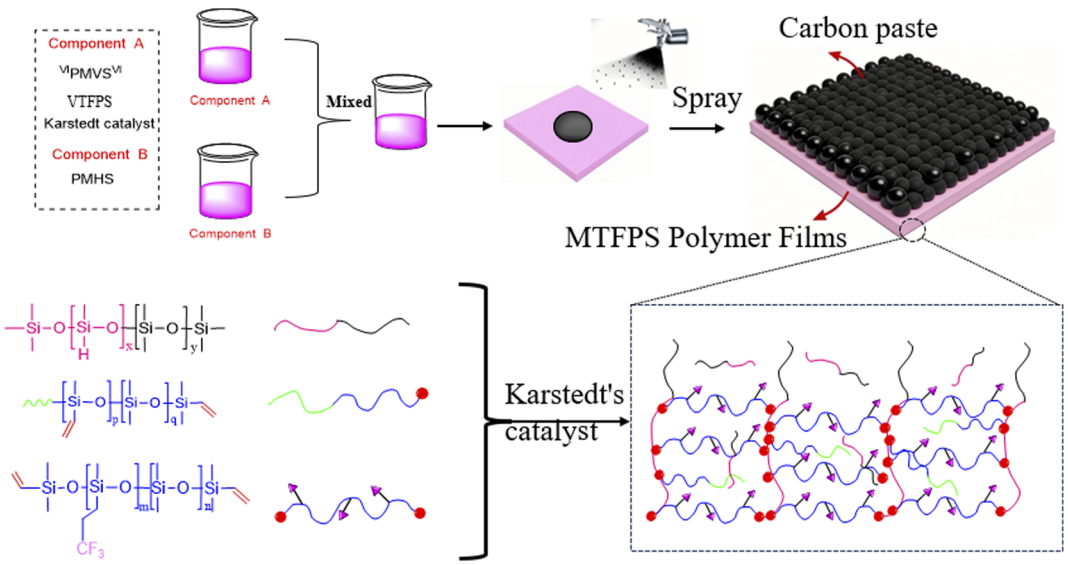

Fig. 19 Schematic of the fabrication process of MTFPS synthetic leather for wearable sensing devices.

and stirred thoroughly, after which the mixture was blade-coated onto release paper using a coating bar to obtain an organic fluorosilicone polymer layer.

The carbon paste was dissolved in dichloromethane (CH_2Cl_2) and spray-coated onto the surface of the organic fluorosilicone polymer at the semi-cured stage, followed by complete curing at room temperature. Subsequently, a silicone adhesive was applied, and after the adhesive became semi-dry, the MTFPS polymer coating was laminated with the base fabric and heated in an oven. Finally, the release paper was peeled off to obtain the wearable sensing device, MTFPS synthetic leather.

Conclusions

In this study, MTFPS synthetic leather was successfully prepared *via* an *in situ* hydrosilylation method using ^{Vi}PMVS^{Vi}, PMHS, VTFPS, and conductive carbon paste, with a platinum complex as the catalyst under a thermally induced catalytic system. The effects of different fluorosilicone oil contents on the properties of the silicone-based synthetic leather were investigated. When the fluorosilicone oil content was 6 wt%, MTFPS synthetic leather exhibited optimal performance: the elongation at break increased from 163.35% to 296.25%, tensile strength rose from 9.93 MPa to 14.83 MPa, and air permeability, water vapor transmission, and tear strength reached 74.62 mL $(cm^2\ h)^{-1}$, 0.016 mg $(cm^2\ h)^{-1}$, and 56.89 N mm^{-1}, respectively. The contact angles at room temperature and low-temperature increased from 105.6° and 109.9° to 128.3° and 130.1°, respectively. Compared with PU and PVC synthetic leathers, the prepared MTFPS synthetic leather demonstrated excellent low-temperature flexibility (−80 °C), wear resistance (30 000 cycles), flexural endurance (30 000 cycles), hydrophobicity (>90°), and anti-graffiti performance under both dry and wet conditions. By incorporating conductive materials into the synthetic leather, the MTFPS polymer exhibits excellent properties, including a wide strain range (0.5–20%), high strain sensitivity (50–250 mm min^{-1}), rapid response speed (0.11 s), good long-term stability, outstanding durability (200 stretch–release cycles), and excellent flexibility and conductivity even at low-temperatures. To further validate the structural origin of the above performance, additional interfacial, mechanical, and morphological characterizations were carried out. The results show that the MTFPS-9/C system forms a robust composite structure with strong interfacial adhesion, as confirmed by peeling tests and cross-sectional SEM observations. The incorporation of conductive carbon slightly decreases tensile strength but enhances elongation at break, indicating improved toughness and flexibility. Notably, the mechanical properties are well maintained at −80 °C, demonstrating excellent low-temperature mechanical stability. SEM analysis reveals that the pristine MTFPS-9 exhibits a porous structure, while the carbon-modified system forms a continuous conductive network. Under tensile deformation, microcracks are generated and propagated, which dynamically regulate conductive pathways and govern the electromechanical response. Importantly, similar crack evolution behaviour is observed at room temperature and −80 °C, indicating that the material maintains structural integrity without significant brittle fracture under low-temperature conditions. In addition, the material exhibits excellent durability and flexibility, as demonstrated by stable resistance responses over 200 stretch–release cycles and good structural integrity after 30 000 folding cycles at both room temperature and −80 °C. Overall, the combination of a flexible fluorosilicone matrix, robust interfacial adhesion, and a stable conductive network enables the MTFPS system to achieve superior mechanical, electrical, and environmental stability. These characteristics make it highly promising for applications in flexible wearable sensing devices, such as health monitoring, human motion detection, soft robotics, electronic skin, and human–machine interfaces, providing an effective strategy to address the challenge of low-temperature brittleness in flexible electronics.

Conflicts of interest

There are no conflicts to declare.

Data availability

The authors confirm that the data supporting the findings of this study are available within the article and supplementary information (SI). Supplementary information: the ^{1}H NMR spectrum of VTFPS, bending resistance performance at 25 °C and −80 °C, air and water vapor permeability data, and tearing strength performance data of MTFPS synthetic leather with different fluorosilicone oil contents. See DOI: https://doi.org/10.1039/d6ra02458k.

Acknowledgements

The authors are grateful for the financial support of National Natural Science Foundation of China (No. 22078165 and 21978139); Shandong Provincial Natural Science Foundation (No. ZR2020QB112); Young Doctoral Innovation Funds (2022PX062) of Qilu University of Technology.

Notes and references

1 X. Liu, Y. Wei and Y. Qiu, *Micromachines*, 2021, **12**, 695.
2 Y. Huang, Y. Xiang, W. Ren, F. Li, C. Li and T. Yang, *Sci. China Technol. Sci.*, 2021, **64**, 1805–1813.
3 W. Asghar, F. Li, Y. Zhou, Y. Wu, Z. Yu, S. Li, D. Tang, X. Han, J. Shang, Y. Liu and R.-W. Li, *Adv. Mater. Technol.*, 2020, **5**, 1900934.
4 P. Makushko, E. S. Oliveros Mata, G. S. Cañón Bermúdez, M. Hassan, S. Laureti, C. Rinaldi, F. Fagiani, G. Barucca, N. Schmidt, Y. Zabila, T. Kosub, R. Illing, O. Volkov, I. Vladymyrskyi, J. Fassbender, M. Albrecht, G. Varvaro and D. Makarov, *Adv. Funct. Mater.*, 2021, **31**, 2101089.
5 C. Yan, Z. Chen, H. Deng, H. Huang and X. Deng, *J. Energy Chem.*, 2023, **80**, 758–767.
6 A. Ranka, M. Layek, S. Kochiyama, C. López-Pernia, A. M. Chandler, C. A. Kocoj, E. Magliano, A. Di Carlo,

F. Brunetti, P. Guo, S. Suresh, D. C. Paine, H. Kesari and N. P. Padture, *npj Flexible Electron.*, 2025, **9**, 92.
7 L. Li, L. Han, H. Hu and R. Zhang, *Mater. Adv.*, 2023, **4**, 726–746.
8 A. Malik and B. Kandasubramanian, *Polym. Rev.*, 2018, **58**, 630–667.
9 H. Song, J. Ma, C. Li, Y. Cai, Y. Wang, X. Cheng, Z. Li, C. Long, C. Liu and Y. Qing, *Chem. Eng. J.*, 2024, **481**, 148346.
10 Y. Liu, X. Li, H. Yang, P. Zhang, P. Wang, Y. Sun, F. Yang, W. Liu, Y. Li, Y. Tian, S. Qian, S. Chen, H. Cheng and X. Wang, *ACS Nano*, 2023, **17**, 5588–5599.
11 Z. Zhang, Q. Zhang, Z. Xia, J. Wang, H. Yao, Q. Shen and H. Yang, *Nano Energy*, 2023, **109**, 108300.
12 P. Wang, W. Wei, Z. Li, W. Duan, H. Han and Q. Xie, *J. Mater. Chem. A*, 2020, **8**, 3509–3516.
13 X. Zhou, Z. Zhai, J. Wang, T. Wang, H. Zheng, Y. Wu, C. Yan and M. Liu, *ACS Appl. Polym. Mater.*, 2024, **6**, 7137–7147.
14 Y. Wang, W. Cai, Y. Zhang, J. Ji, H. Zheng, D. Yan and X. Liu, *Discover Nano*, 2024, **19**, 176.
15 X. Zeng, H. Ong, L. Haworth, Y. Lu, D. Yang, M. Rahmati, Q. Wu, H. Torun, J. Martin, X. Hou, X. Lv, W. Yuan, Y. He and Y. Fu, *ACS Appl. Mater. Interfaces*, 2023, **15**, 35648–35663.
16 İ. Baylakoğlu, A. Fortier, S. Kyeong, R. Ambat, H. Conseil-Gudla, M. H. Azarian and M. G. Pecht, *e-Prime – Adv. Electr. Eng. Electron. Energy*, 2021, **1**, 100016.
17 Z. Yao, H. Feng, K. Shang, X. Deng and T. Yang, *ACS Appl. Nano Mater.*, 2023, **6**, 6550–6558.
18 C. Xiao, X. Liu, Y. Zhao, C. Huang, N. Zhou and H. Mao, *Microsyst. Nanoeng.*, 2025, **11**, 221.
19 Z. Liu, J. Liu, J. Zhang, B. Zheng, X. Ren, Y. Long, L. Fang, R. Ou, T. Liu and Q. Wang, *Mater. Chem. Front.*, 2020, **4**, 3319–3327.
20 M. Xia and Q. Shi, *Micromachines*, 2024, **15**, 1350.
21 Z. Sun, J. Wen, W. Wang, H. Fan, Y. Chen, J. Yan and J. Xiang, *Prog. Org. Coat.*, 2020, **146**, 105744.
22 Z. Yang, Y. Bai, L. Meng, Y. Wang, A. Pang, X. Guo, J. Xiao and W. Li, *Eur. Polym. J.*, 2022, **163**, 110903.
23 J. I. So, C. S. Lee, J. Y. Jung, J. Lee, J. K. Choi, S. E. Shim and Y. Qian, *Polymers*, 2022, **14**, 5502.
24 Q. Song, A. Hamza, C. Li, A. S. Sedeky, Y. Chen, M. Zhu, A. Goralczyk, F. Mayoussi, P. Zhu, P. Hou, C. Piesold, D. Helmer, B. E. Rapp and F. Kotz-Helmer, *Addit. Manuf.*, 2024, **81**, 103991.
25 Y.-W. Park, J.-H. Yoon, K.-H. Shin, Y.-J. Cho, J.-H. Yun, W.-H. Han, M.-H. Hong, D.-G. Kang and H.-Y. Kim, *Polymers*, 2023, **15**, 4489.
26 Y. Xing, H. Kang, D. Li, F. Yang and Q. Fang, *Polym. Degrad. Stab.*, 2024, **230**, 111034.
27 Z. Wang, Y. Lin, Z. Li, Y. Yang, J. Lin and S. He, *Polymers*, 2023, **15**, 3448.
28 Q. Zhang and M. Wu, *J. Appl. Polym. Sci.*, 2024, **141**, e55642.
29 Y. Yu, S. Wang, H. Yu, X. Liao and W. Feng, *Mater. Horiz.*, 2025, **12**, 2679–2688.
30 W. Chen, Z. Li, F. Zou, J. Yu, C. Li, X. Zhang and J. Guo, *New J. Chem.*, 2026, **50**, 3306–3319.
31 H.-J. Men, B.-J. Huang and J.-C. Li, *ACS Appl. Mater. Amp. Interfaces*, 2024, **16**, 7489–7499.
32 L. Li, H. Zheng, Z. Xia, Z. Feng, X. Hou, J. He, Y. Yan, Z. Niu and C. Bai, *Macromolecules*, 2025, **58**, 4746–4757.
33 Y. Zhao, H. Ma, J. Shi, X. Yang, D. Zha, X. Tan, Q. Hu, X. Xie, X. Wang, Y. Cai, X. Gong, R. Liu and W. Peng, *J. Phys., Conf. Ser.*, 2025, **3009**, 012015.
34 F. Yang, L. Peng, Y. Huang, J. Li, W. Chen, L. Zhao, J. Gao, Y. Shi, K. Cao, Z. Chen, G. Zhang and L. Tang, *ACS Sens.*, 2025, **10**, 7278–7290.
35 S. Mesa, E. Ramírez, K. G. Rivera Botia, F. Jaramillo and D. Ramírez, *Sci. Rep.*, 2025, **15**, 6397.
36 Y. Qin, X. Ouyang, Y. Lv, W. Liu, Q. Liu and S. Wang, *Coatings*, 2023, **13**, 1769.
37 P. Cataldi, D. G. Papageorgiou, G. Pinter, A. V. Kretinin, W. W. Sampson, R. J. Young, M. Bissett and I. A. Kinloch, *Adv. Electron. Mater.*, 2020, **6**, 2000429.
38 J. Xie, J. Hu, X. Lin, L. Fang, F. Wu, X. Liao, H. Luo and L. Shi, *Appl. Surf. Sci.*, 2018, **457**, 870–880.
39 O. Akin and F. Temelli, *Desalination*, 2011, **278**, 387–396.
40 T. D. Blake and G. N. Batts, *J. Colloid Interface Sci.*, 2019, **553**, 108–116.
41 J. Wen, Z. Sun, J. Xiang, H. Fan, Y. Chen and J. Yan, *Appl. Surf. Sci.*, 2019, **494**, 610–618.
42 W. Yang, X. Du, Z. Du, H. Wang and X. Cheng, *J. Appl. Polym. Sci.*, 2019, **136**, 47167.
43 S. Wang, S. Tang, C. He and Q. Wang, *Polymers*, 2023, **15**, 899.
44 S. A. R. Naga and T. A. El-Sayed, *J. Fail. Anal. Prev.*, 2024, **24**, 922–935.
45 X. Zhang, N. Li, G. Wang, C. Zhang, Y. Zhang, F. Zeng, H. Liu, G. Yi and Z. Wang, *RSC Adv.*, 2023, **13**, 16693–16711.